J Mol Model (2015) 21: 21
DOI 10.1007/s00894-015-2577-5

ORIGINAL PAPER

Theoretical predictions of thermodynamic parameters of adsorption of nitrogen containing environmental contaminants on kaolinite

Andrea Michalkova Scott · Elizabeth A. Burns · Brandon J. Lafferty · Frances C. Hill

Received: 12 October 2014 / Accepted: 7 January 2015 / Published online: 27 January 2015

Abstract In this study thermodynamic parameters of adsorption of nitrogen containing environmental contaminants (NCCs, 2,4,6, trinitrotoluene (TNT), 2,4-dinitrotoluene (DNT), 2,4-dinitroanisole (DNAN), and 3-one-1,2,4-triazol-5-one (NTO)) interacting with the tetrahedral and octahedral surfaces of kaolinite were predicted. Adsorption complexes were investigated using a density functional theory and both periodic and cluster approach. The complexes, modeled using the periodic boundary conditions approach, were fully optimized at the BLYP-D2 level to obtain the structures and adsorption energies. The relaxed kaolinite-NCCs structures were used to prepare cluster models to calculate thermodynamic parameters and partition coefficients at the M06-2X-D3 and BLYP-D2 levels from the gas phase. The entropy effect on the Gibbs free energies of adsorption of NCCS on kaolinite was also studied and compared with available experimental data. The results showed that in all calculated models, the NCCs molecules are physisorbed and they favor a parallel orientation toward both kaolinite surfaces. It was found that all calculated NCCs compounds are more stable on the octahedral than on the tetrahedral surface of kaolinite. The Gibbs free energies and partition coefficients were also predicted for interactions of NCCs with Na-kaolinite from aqueous solution. Calculations revealed adsorption of NCCs is effective from the gas phase on both cation free kaolinite surfaces and on Na-kaolinite from aqueous solution at room temperature. Theoretical data were validated against experimental results, and the reasons for small differences between calculated and measured partition coefficients are discussed.

Keywords Binding · Clay · Distribution · Modeling · Nitroaromatic

Electronic supplementary material The online version of this article (doi:10.1007/s00894-015-2577-5) contains supplementary material, which is available to authorized users.

A. M. Scott (✉) · B. J. Lafferty · F. C. Hill
U. S. Army Engineer Research and Development Center (ERDC), 3909 Halls Ferry Rd., Vicksburg, MS 39180, USA
e-mail: andrea.m.scott@usace.army.mil

E. A. Burns
Badger Technical Services, LLC, 3909 Halls Ferry Rd., Vicksburg, MS 39180, USA

Introduction

Nitrogen containing compounds (NCCs) including nitroaromatic compounds (NACs, 2,4,6, trinitrotoluene (TNT), 2,4-dinitrotoluene (DNT), 2,4-dinitroanisole (DNAN)) and 3-one-1,2,4-triazol-5-one (NTO), widely used as explosives, have received considerable attention due to their environmental impact as contaminants. A few experimental papers have been published on adsorption of NACs on kaolinite in the presence of cations [1–8]. An electron donor-acceptor (EDA) complex was suggested to be the governing mechanism of adsorption of NACs on the siloxane surface. The strength of adsorption was shown to depend on the structure of the compound (type of substituent) and on the type of cation on the siloxane surface [2]. Distribution coefficients (K_d) have also been measured, and the highest values were found for polynitroaromatic compounds (e.g., TNB, TNT) [1].

Adsorption processes occurring on soil mineral surfaces (dry or hydrated) play a crucial role in determining the fate and distribution of organic contaminants in the environment. Thus, investigations of surface adsorption sites on soil components (e.g., clay minerals), the binding nature and sorption mechanisms of contaminants on soil minerals are crucial to

understand sorption phenomena in soils. Clay minerals are one of the most chemically dominant components of soil that significantly affect the fate and transport of organic chemicals. Minerals of the kaolinite group have been reported to adsorb various munitions-related nitroaromatic compounds (NACs) such as 2,4-dinitrotoluene (DNT) [9, 10], nitrobenzene (NB) [11], 1,3-dinitrobenzene, 1,3,5-trinitrobenzene (TNB) [12–14], as well as different derivatives of nitrotoluene and nitrophenol [2–7]. Kaolinite is a dioctahedral layered 1:1 aluminosilicate ($Al_2Si_2O_5(OH)_4$), with layers consisting of an octahedral sheet (formed of AlO_6 octahedra), and tetrahedral sheet (formed of SiO_4 tetrahedra) [15, 16]. The Al octahedra and Si tetrahedra are connected with each other through the oxygen centers to form layers, and the layers are bound to each other via hydrogen bonds formed between the hydroxyl groups of the octahedral sheet to the basal oxygen atoms of the tetrahedral sheet [17]. Moreover, the ideal structure of kaolinite is electroneutral (the interlayer space does not contain any exchangeable cations, and there are no substitutions in the layers). Thus, in our study kaolinite was selected to create the surface models to study the adsorption phenomenon on clay minerals.

First, we will summarize the results of computational studies on adsorption of nitrogen containing environmental contaminants on clay mineral surfaces. A few of these papers have focused on interactions between NACs adsorbed on kaolinite or montmorillonite [9–13, 17], in which the mineral surface models were prepared using the cluster approach. The periodic approach has been applied only once to calculate the adsorption of TNB and 1,3,5-trinitro-1,3,5-triazacyclohexane (RDX) [18]. To the best of our knowledge, adsorption of target NCCs by both kaolinite surfaces (i.e., octahedral and tetrahedral surfaces) was investigated theoretically in only one study using the cluster approach at the M06-2X level [19]. In this study, the structure, interactions, and binding energies of NCCs adsorbed on the tetrahedral and octahedral kaolinite surfaces were investigated [19]. The main conclusion of the above listed publications [9–13, 17–19] is that the cluster approach is insufficient to treat accurately complex phenomena of adsorption on clay minerals. The methods, without inclusion of long-term dispersion, were shown to underestimate the interaction energies of NACs on the kaolinite surfaces [19]. HF, DFT(B3LYP), and MP2 methods were not able to correctly predict interaction energies for adsorption systems when small cluster models of the mineral surface were used [12, 13]. DFT functionals, developed to take into account both short- and long-term dispersion interactions, have been shown to accurately produce adsorption energies for various aromatic compounds interacting with minerals and metal oxides [20, 21]. However, Gibbs free energies of adsorption on the kaolinite surfaces have not been predicted for both, the gas phase and aqueous solution. The main reason is that such studies are time-consuming especially if one wants to obtain accurate results when compared with experimental data. A few theoretical studies have been recently published to better understand thermodynamics of adsorption processes on soil components from the gas phase and aqueous solution [22–27]. They include publications on adsorption of polycyclic aromatic hydrocarbons (PAHs) and NCCs on carbon black [25–27]. In these studies different approaches were investigated to accurately predict thermodynamic parameters and partitioning coefficients for carbon-NCCs and carbon-PAHs that can be applied to other sorption systems on soil components.

The aim of this study is to investigate adsorption of selected NCCs on the surface models of kaolinite from vacuum. This work will predict the binding geometries and interaction energies of the kaolinite-NCCs (K-NCCs) systems. The ultimate goal is to predict the Gibbs free energies of adsorption and partition coefficients for distribution of selected explosives between kaolinite and air. The cluster and periodic approaches will be applied to model the kaolinite-NCCs adsorption systems. This investigation is a part of an ongoing research to develop a computational strategy to accurately characterize the fate of organic contaminants in the environment with a limited amount of experimental data, and test reliability and effectiveness of used modeling approaches.

Computational details

The combined modeling approximation was applied to study adsorption of NCCs on kaolinite surfaces as follows: in the first step, the kaolinite-NCCs systems modeled using the periodic boundary conditions (PBC) approach were fully relaxed to obtain the optimized geometries and adsorption energies; in the second step, the PBC kaolinite-NCCs optimized structures were used to construct the kaolinite-NCCs cluster models to calculate adsorption entropies, enthalpies, Gibbs free energies, and partition coefficients. It has been shown that this method provides adsorption energies and enthalpies with an almost experimental accuracy [25, 26].

Periodic approach

The crystal structure of kaolinite was used to prepare the periodic models of the octahedral and tetrahedral surface of kaolinite [28]. The experimental lattice parameters were: a= 5.154 Å, b=8.942 Å, c=7.401 Å, α=91.69°, β=104.61°, and γ=89.82°. The axes of the unit cell are oriented so that the (001) plane corresponds to the octahedral and tetrahedral basal surfaces, respectively. The conventional $Al_4Si_4O_{10}(OH)_8$ unit cell was employed for structure optimizations of the kaolinite bulk, with full relaxations of all atoms within the box. The calculated unit cell consists of a (3x2) slab of kaolinite to ensure that interactions of adsorbates with their

periodic images in the *a*-*b* plane are minimal. The bulk model of kaolinite has the following dimensions: a=15.462 Å, b= 17.884 Å, c=22.401 Å since 15 Å was added in the c direction to prevent interactions of the adsorbates with the periodic image of the kaolinite layer in the c direction. The kaolinite slab model was comprised of a single kaolinite layer consisting of six full silicon-oxygen tetrahedral rings and six full aluminum-oxygen octahedral rings containing 204 atoms ($Si_{24}Al_{24}O_{60}(OH)_{48}$). This unit cell was used to investigate the gas phase adsorption of NCCs on the (001) surfaces of kaolinite. The (3x2) slab size of the periodic kaolinite model was found to be reliable to study adsorption of various organic chemicals (including TNB and RDX [18]) on the surfaces of kaolinite (see for example 29, 30). The inner and outer OH groups bonded with the aluminum atoms in the octahedral sheet of the periodic kaolinite models were initially orientated according to the results for the geometry of kaolinite bulk [31–33]. Selected NCCs were adsorbed on both surfaces of this kaolinite model in a parallel (we will use notation K-NCCs (=)) or perpendicular (we will use notation K-NCCs(⊥)) way. Several different initial orientations of NCCs toward both surfaces were examined.

The periodic DFT calculations were performed using the Car-Parrinello molecular dynamics (CPMD) code [34]. A plane-wave basis set and the BLYP exchange-correlation functional [35, 36] with inclusion of the D2 dispersion correction were used for the total-energy geometry optimization of kaolinite-NCCs periodic models. The D2 correction was incorporated to reproduce long-range dispersion contributions using the Grimme's empirical method [37]. This method is based on the addition of the C_6R^{-6} form of pairwise interatomic potentials to the conventional Kohn−Sham DFT energy. The Kleinman-Bylander separation scheme and Goedecker-Teter-Hutter (GTH) pseudopotentials were applied to mimic the effect of the inner electrons for all atoms [38, 39]. The form of GTH pseudopotentials has been optimized to efficiently perform real-space DFT calculations. The plane-wave kinetic energy cutoff was set to 952 eV, respectively. The Γ-point sampling was restricted for the Brillouin-zone integration. The kaolinite-NCCs PBC models were fully optimized until the Hellmann-Feynman forces were less than 0.05 eV/Å, and the error in the total energy convergence was less than 10^{-6} eV. All of the atomic positions were allowed to relax, but the shape and size of the computational unit cells were conserved.

Cluster approach

The density functional theory (DFT) [40] and 6-31+G(d,p) basis set were applied, and the E.01 version of Gaussian09 [41] was employed. Calculations of kaolinite-NCCs cluster models were performed using two different DFT functionals (BLYP [35, 36] and M06-2X [42]). In order to compare the effect of dispersion interactions on the adsorption energies of the kaolinite-NCCs systems, BLYP and M06-2X were incorporated with two different Grimme's dispersion correction terms (D2 [37] and D3, in which the C_6 term is no longer scaled [43]). The studied systems were allowed to fully relax. Vibrational frequency calculations were carried out to verify that the true minima were obtained from the geometry optimization for all studied kaolinite-NCCs systems.

The cluster models were applied to calculate adsorption enthalpies (ΔHads), Gibbs free energies (ΔGads) and partition coefficients (log K_d, they characterize distribution of selected contaminants between kaolinite and air) for all studied K(o)-NCCs and K(t)-NCCs systems at room temperature from the gas phase. The basis set superposition error (BSSE) correction was also included at these levels of theory using the counterpoise method [44]. The adsorption entropy values (TΔSads) were calculated using the rigid rotor – harmonic oscillator – ideal gas approximation based on the harmonic vibrational frequencies at 298.15 K and 1 atm pressure.

The kaolinite-NCCs cluster models were prepared as cut outs from the PBC optimized geometries of kaolinite-NCCs systems calculated at the BLYP-D2 level so that they contain one tetrahedral ring of the tetrahedral sheet, one octahedral ring of the octahedral sheet, and one NCC molecule. The kaolinite cluster models have the $Al_6Si_6O_{36}H_{30}$ chemical formula, and they were composed from six SiO_4 tetrahedra, which share corners, and six AlO_6 octahedra, sharing edges. Dangling bonds of the cluster models were saturated with hydrogen atoms to ensure electroneutrality of the system. The following conventions will be used in the text, tables and Figures for the kaolinite-NCCs models: K(o)-NCCs and K(t)-NCCs for adsorption systems of NCCs on the octahedral and tetrahedral surface of kaolinite, respectively.

Results and discussion

Geometry of adsorption complexes

Optimized structures of all calculated NCCs (DNT, DNAN, NTO, and TNT) adsorbed on the octahedral (K(o)-NCCs) and tetrahedral surfaces (K(t)-NCCs) of kaolinite obtained at the BLYP-D2(PBC) level are illustrated in Figs. 1, 2, 3, 4, 5, 6, 7 and 8. The geometry of the K(o)-NCCs and K(t)-NCCs adsorption complexes has already been described in detail in our previous study [19]. Therefore, in this section we will focus on the main differences in optimized geometries of kaolinite-NCC systems with NCCs oriented in a parallel way toward the surface (K-NCCs(=)) obtained at the BLYP-D2(PBC) and M06-2X(Cluster) levels [19]. In addition, optimized structures of the kaolinite-NCCs systems with NCCs oriented in a perpendicular way toward the kaolinite surface (K-NCCs(⊥)) will be briefly discussed.

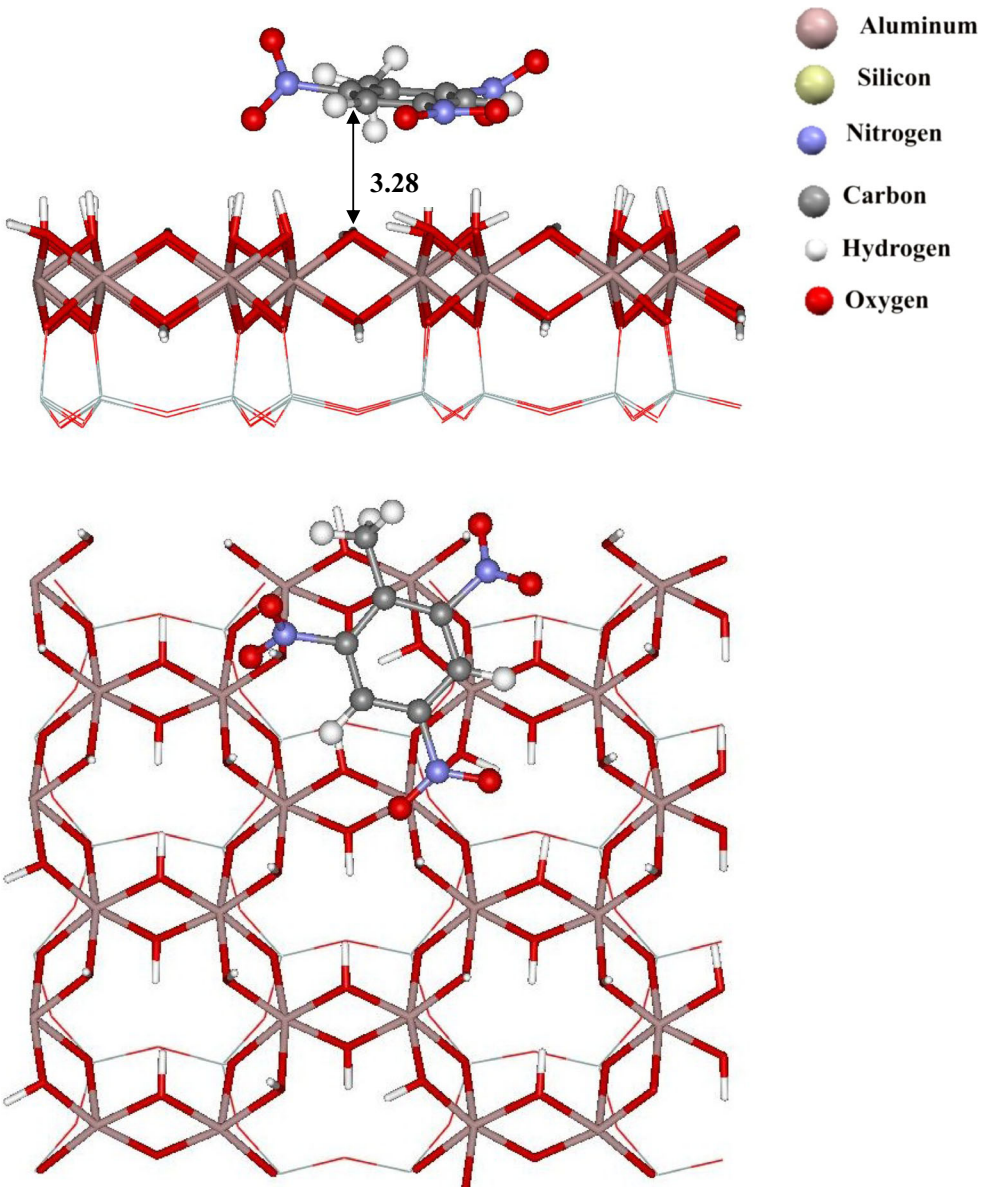

Fig. 1 Top and side view of the optimized structure of TNT adsorbed in a parallel orientation toward the octahedral kaolinite surface (K(o)-TNT(=)) obtained at the BLYP-D2(PBC) level of theory

All NACs are placed in a coplanar orientation on both kaolinite surfaces (Figs. 1, 2 and 3), which is in good agreement with previous experimental and theoretical findings [1–8, 11–13, 18, 19]. An exception is K(o)-NTO where NTO is oriented toward the surface by the N1-H group in an angle of 50° (see Fig. 4). The BLYP-D2(PBC) vertical distances between the aromatic ring of NCCs and the plane of the octahedral surface oxygen atoms are in a range 2.88-3.28 Å in K(o)-NCC(=). In K(t)-NCC(=), distances between the adsorbate and plane of the basal oxygen atoms of the tetrahedral surface vary between 2.9 and 3.13 Å. Adsorption of the NCCs molecules on the PBC model of the octahedral kaolinite surface is governed by multiple hydrogen bonds, while adsorption on K(t) is mostly controlled by dispersion forces. This is in accordance with the results of previous studies of adsorption of TNB and NB on the siloxane surface [12, 13, 18]. The main difference between the kaolinite-NCC optimized structures obtained using the PBC and cluster approach (M06-2X-D3, BLYP-D2) calculated in this and previous study (M06-2X) [19] is that only K-NCC(=) are found to be stable using the cluster kaolinite models. For K-NCCs(=), the cluster and BLYP-D2(PBC) calculations show almost the same adsorbate-adsorbent binding. The PBC K(t)-NCCs(=) structures confirm that the O…H-O H-bonds found between NCCs and the edge OH groups of the K(t) cluster model in our previous study [19] are only artifacts of the modeling approach, and they do not exist in real systems. The reason is that the full optimization of the K(t) model changes orientation of hydrogen atoms of edge OH groups so that one or two of these edge OH groups form H-bonds with the adsorbate. These hydrogen atoms have been added only to saturate dangling bonds of the K(t) model (do not exist in the real system).

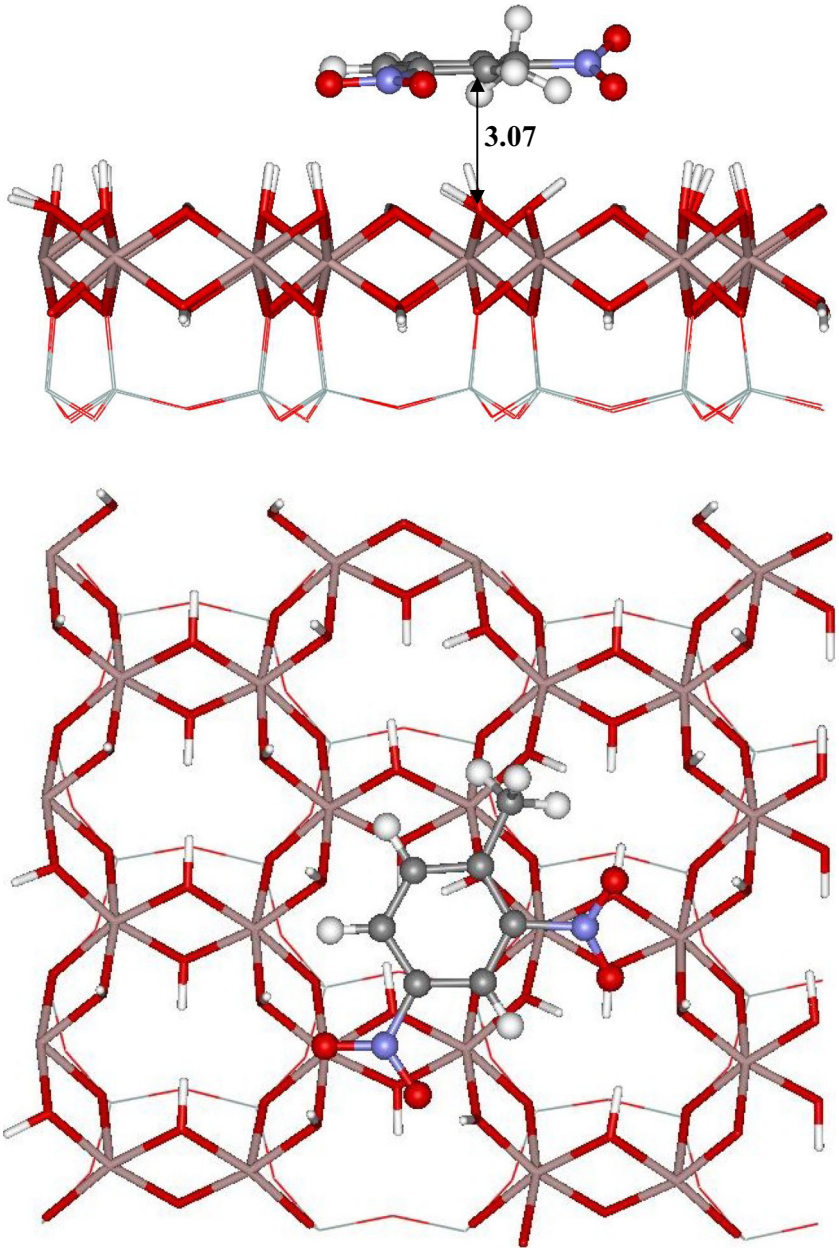

Fig. 2 Top and side view of the optimized structures of DNT adsorbed in a parallel orientation toward the octahedral kaolinite surface (K(o)-DNT(=)) obtained at the BLYP-D2(PBC) level of theory

H-bonds between the K(t) mode and adsorbate, in which these hydrogen atoms participate, are therefore an artifact of the model (see ref 19 for more explanation).

Figures S1-S6 in the Supporting Information illustrate the optimized geometries of the kaolinite–NACs systems with NACs placed in a perpendicular orientation toward the surface (K-NACs(⊥)) as obtained at the BLYP-D2(PBC) level. In K-NACs(⊥), NACs are oriented toward the surface in almost perpendicular orientation with only a small leaning (by less than 5°). The full relaxation of K(o)-NTO(⊥) and K(t)-NTO(⊥) has led to the same structures as revealed from the optimization of K(o)-NTO(=) and K(t)-NTO(=) (Figs. 4 and 8). This means that only K-NTO complexes with NTO tilted toward both kaolinite surfaces at an angle of 50° are stable. Thus, only this type of the kaolinite-NTO systems were further analyzed and they are denoted K(o)-NTO(=) and K(t)-NTO(=) in the text, Tables and Figures. NACs face the surface by one C3-H and two nitro groups, and NTO by the nitro, N1-H, and C5=O groups. These groups form three O-H…O and one C3-H…O H-bonds (K-NACs(⊥)) with the hydroxyl groups of the octahedral surface or the basal oxygen atoms of the tetrahedral site of kaolinite. Similar binding was found for NACs interacting in a perpendicular orientation with (100) surface of alpha-quartz [20]. The amount and strength of formed H-bonds in all K-NACs(⊥) is smaller than in K-NACs(=).

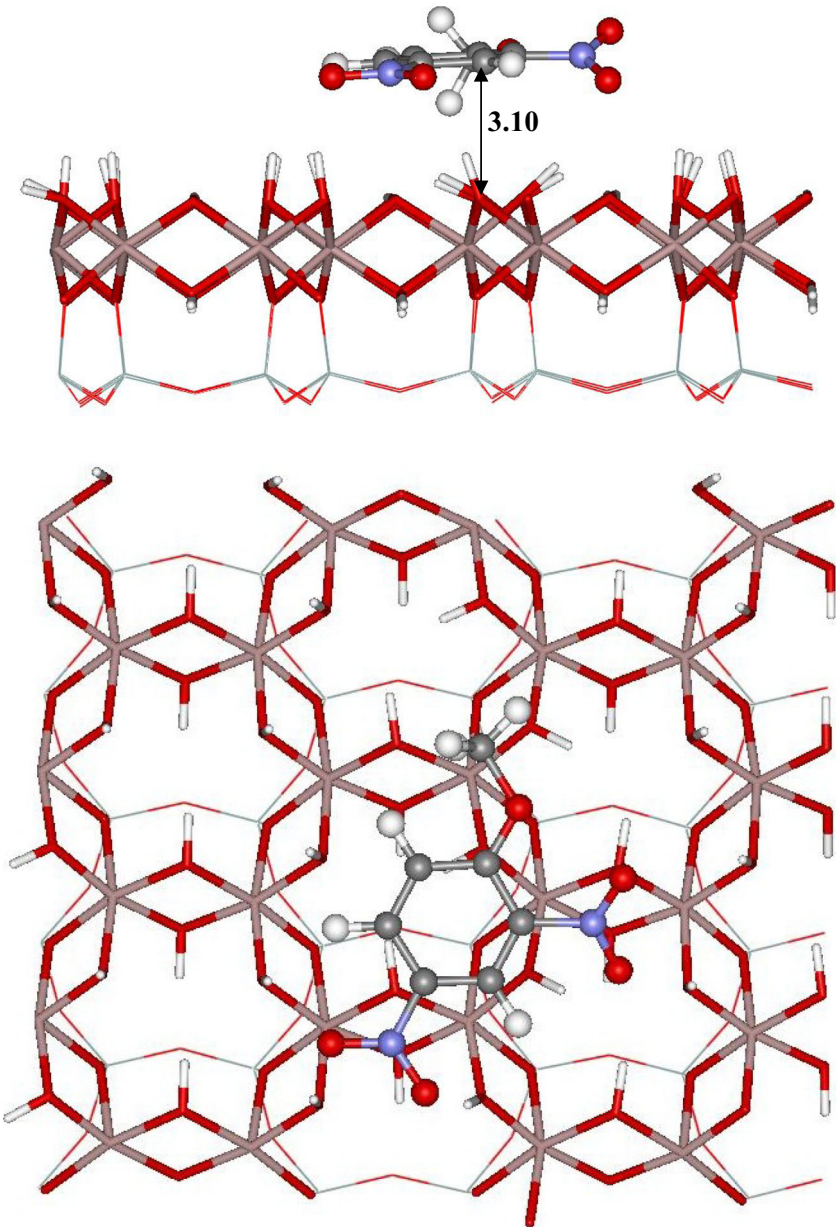

Fig. 3 Top and side view of the optimized structures of DNAN adsorbed in a parallel orientation toward the octahedral kaolinite surface (K(o)-DNAN(=)) obtained at the BLYP-D2(PBC) level of theory

Adsorption energies and enthalpies

The adsorption energies (ΔEads) obtained at all levels used (BLYP-D2(PBC), BLYP-D2(cluster), M06-2X-D3(cluster)) are presented in Table 1. The BSSE values are given in parentheses. These values are much higher at the BLYP-D2 level than at the M06-2X-D3 level. Comparison of the BSSE values obtained at the M06-2X-D3 level with the values from our previous study [19] shows that usage of a larger basis set affects these values more significantly than inclusion of the D3 term.

The PBC results are regarded as more precise when compared with the cluster data due to the application of the nearly complete basis set and interactions of NCCs with virtually infinite surfaces of kaolinite (avoiding artifacts caused by the periodic structure cutout). Therefore, the BLYP-D2(PBC) results are used as our benchmark values, and they are further discussed and compared with the ΔEads values calculated using the cluster approach.

Comparison of the BLYP-D2(PBC) adsorption energies in Table 1 shows that they are more than two times larger for K-NACs(=) (NACs in a parallel orientation toward the surface) than for K-NACs(⊥) (NACs in a perpendicular orientation toward the surface). This implies higher stability of K-NACs(=) than K-NACs(⊥). This result is in accordance with conclusions of previous studies on adsorption of DNT on both kaolinite surfaces [9] and NB and 1,3,5-TNB on the siloxane surface of clay minerals [12, 13]. A parallel

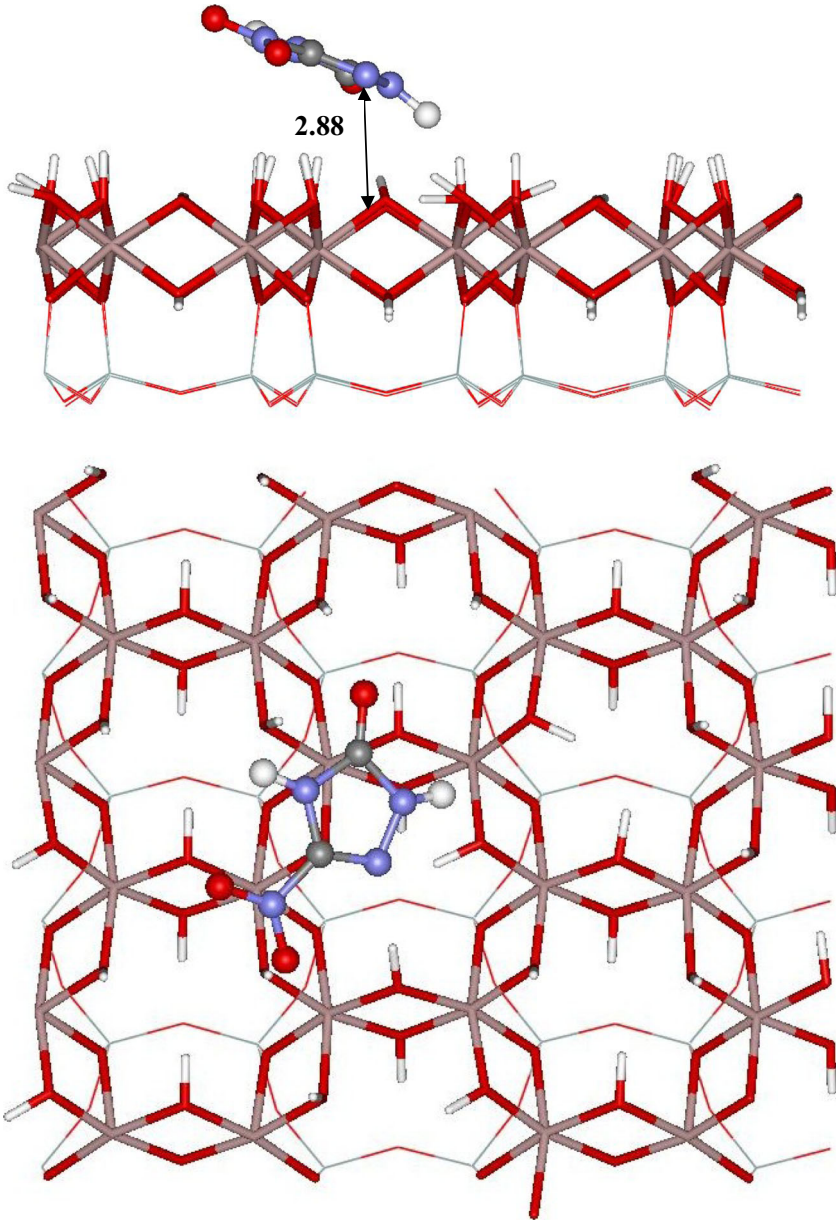

Fig. 4 Top and side view of the optimized structures of NTO adsorbed in a parallel orientation toward the octahedral kaolinite surface (K(o)-NTO(=)) obtained at the BLYP-D2(PBC) level of theory

orientation of NCCs was also revealed to be favorable for adsorption of NCCs on the (100) α-quartz [20], and alumina surface [45, 46]. Energies, enthalpies, entropies, and Gibbs free energies, and partitioning coefficients will further be analyzed only for the more stable kaolinite-NCCs complexes (K-NCCs (=) with a parallel orientation of NCCs toward the surface).

Greater adsorption energies are observed for K(o)-NCCs than K(t)-NCCs at all levels of theory used, with the energy difference of about 10 kcal mol^{-1}, similarly as revealed for DNT [9, 10], benzene (difference of 5 kcal mol^{-1}) [47, 48], and other aromatic molecules (thymine and uracil with difference of 7 and 8 kcal mol^{-1}) [49]. A different trend in the stabilization of NCCs is indicated for the octahedral than for the tetrahedral kaolinite surface. In the K(o)-NCC complexes, the ΔEads value is largest for TNT, followed by DNAN, DNT, and NTO. In the case of K(t)-NCCs, we predict NTO to be the most strongly adsorbed followed by DNAN, DNT, and TNT. This is in agreement with the results of adsorption of NCCs on silica, where silica-NTO was also found to be the most stable and silica-TNT the least stable complex [20].

All previously published ΔEads for NCCs (DNT, TNB, triaminotoluene (TAT)) adsorbed on small models of the octahedral (−5 to −19 kcal mol^{-1} [9, 10, 47, 48, 50]) or siloxane dickite and kaolinite surface (-2.7 to -12.4 [9, 10, 12, 13, 50]) are smaller than our BLYP-D2(PBC) values. This can be caused by the fact that dispersion corrections, which were shown to play a major role in adsorption of aromatic compounds on metal oxides [20, 51–55] and minerals [56], were not included in most of these calculations. Other reasons can be the usage of small basis sets and very small models of mineral surfaces.

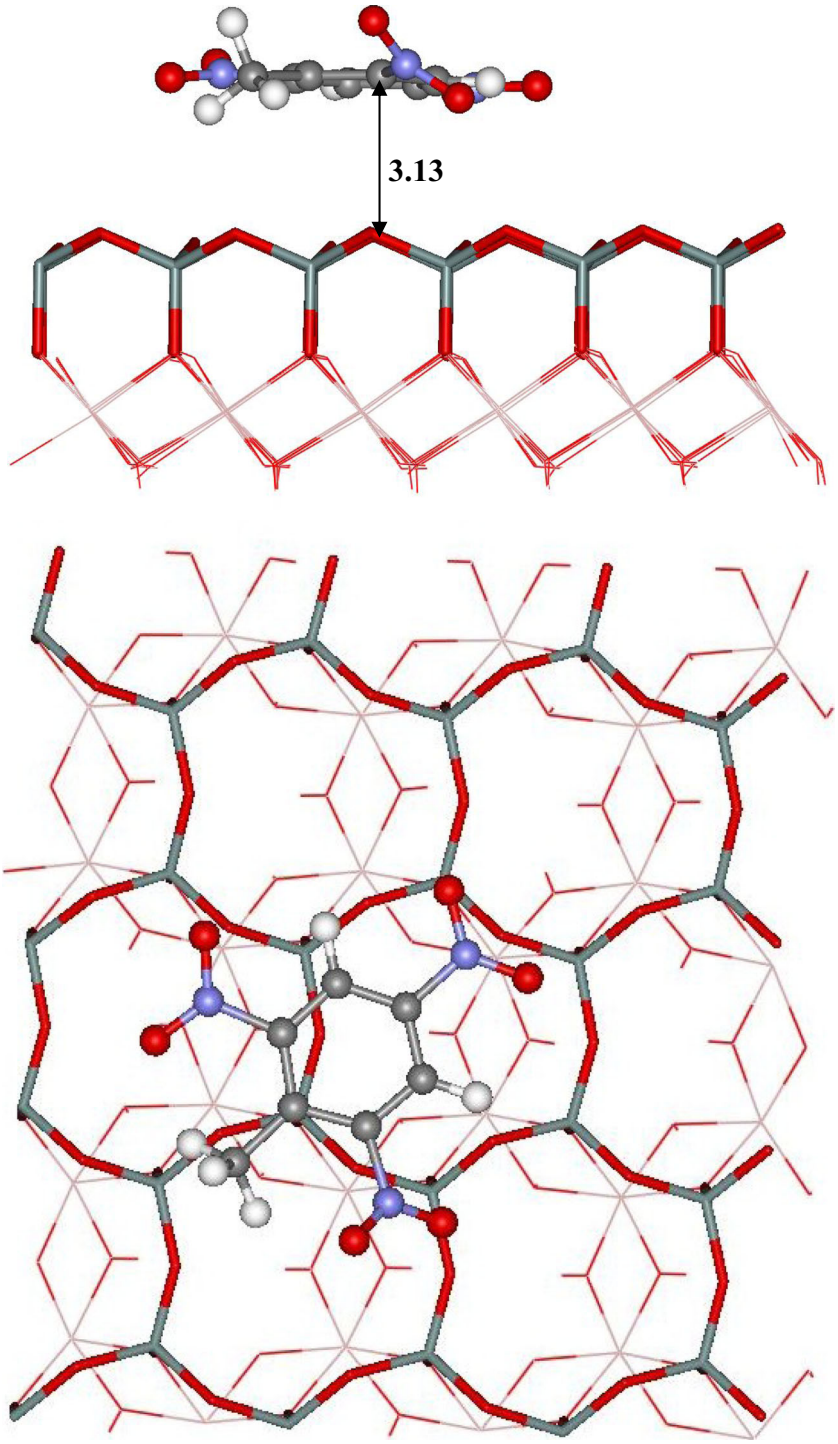

Fig. 5 Top and side view of the optimized structure of TNT adsorbed in a parallel orientation toward the tetrahedral kaolinite surface (K(t)-TNT(=)) obtained at the BLYP-D2(PBC) level of theory

ΔEads obtained using the cluster approach (M06-2X-D3, and BLYP-D2(cluster)) are mostly higher than the BLYP-D2 (PBC) results. They differ by 0.3–3.4 kcal mol^{-1} (M06-2X-D3), and by 1.5–10.8 kcal mol^{-1} (BLYP-D2(cluster)). M06-2X ΔEads data [19] are mostly smaller that the BLYP-D2 and M06-2X-D3 results for K-NCCs. This indicates that long-term dispersion interactions play a role in adsorption of NCCs on both kaolinite surfaces, which varies based on the compound and mineral surface used. One can suggest that the M06-2X-D3 data better mimic data of the PBC model than the BLYP-D2(cluster) results, especially in the case of K(t)-NCCs. Due to a proper account of long-range electron correlation in adsorption on the mineral surfaces, M06-2X-D3 was shown to perform well for a series of compounds [56].

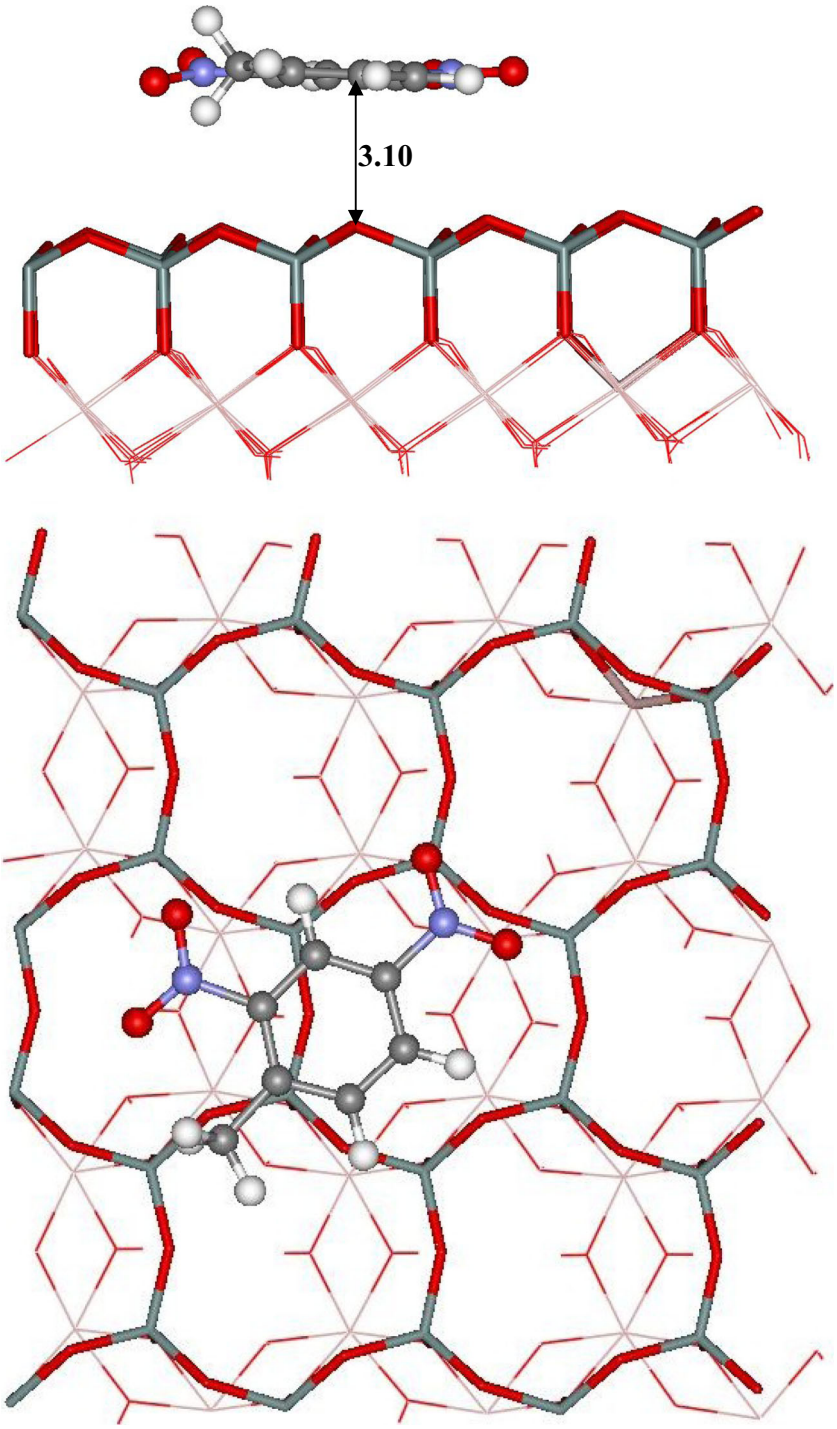

Fig. 6 Top and side view of the optimized structures of DNT adsorbed in a parallel orientation toward the tetrahedral kaolinite surface (K(t)-DNT(=)) obtained at the BLYP-D2(PBC) level of theory

Moreover, several recent benchmarking studies have shown that functionals such as M06-2X-D3 yield higher-quality predictions than MP2 across a broad range of properties [57–60].

There are no experimental adsorption energies available for adsorption of studied NCCs on kaolinite surfaces. Available experimental adsorption enthalpies are for different environmental contaminants (e.g., polychlorinated biphenyls (PCBs)) interacting with soil from air [64, 65]. They amount from −16.9 to −26.1 kcal mol^{-1}. In order to better compare our calculated values with available experimental data, the adsorption enthalpies were calculated for all K-NCCs at all levels used ((BLYP-D2(PBC), M06-2X-D3, BLYP-D2(cluster)), and they are presented in Table 2. The BLYP-D2(PBC) ΔEads values were converted to ΔHads using the zero-point correction obtained at the M06-2X-D3 level since this level was shown to mimic the PBC results most closely. The ΔHads

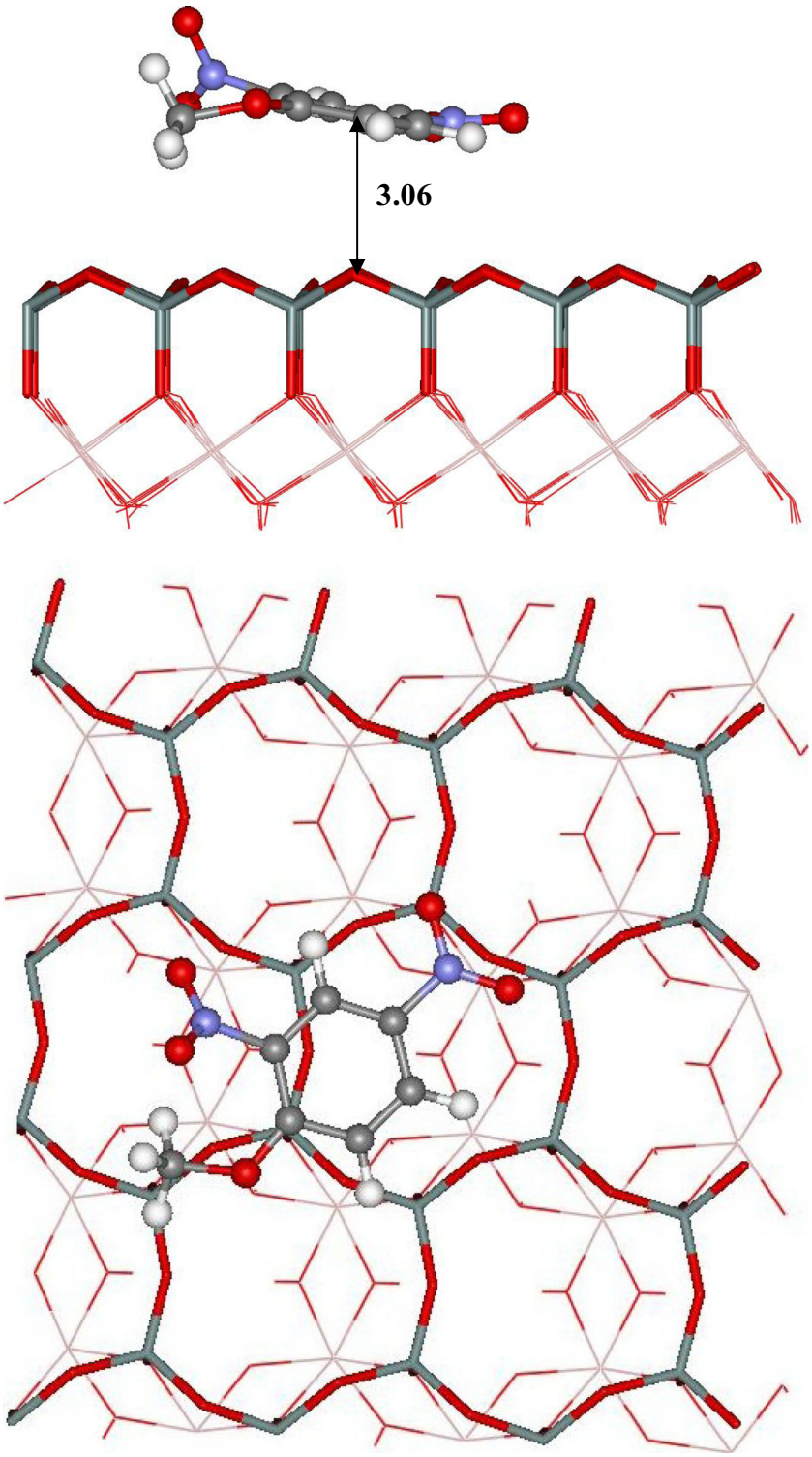

Fig. 7 Top and side view of the optimized structures of DNAN adsorbed in a parallel orientation toward the tetrahedral kaolinite surface (K(t)-DNAN(=)) obtained at the BLYP-D2(PBC) level of theory

values for K(o)-NCCs obtained at all levels considered agree well with the experimentally measured interval indicated above [61, 62].

Only available adsorption enthalpies for compounds related to NCCs were measured for 4-methyl-2-nitrophenol, 3-nitrotoluene, 4-nitrotoluene, 4-chloronitrobenzene, 4-nitrobenzaldehyde adsorbed on the siloxane surface of Cs^+-kaolinite in aqueous solution [1, 2]. Thus, to compare our calculated values with these experimental data, ΔHads of K(t)-NCCs were converted to adsorption enthalpies from aqueous solution (ΔHsol). The fitting was performed based on comparison with previously published theoretical data

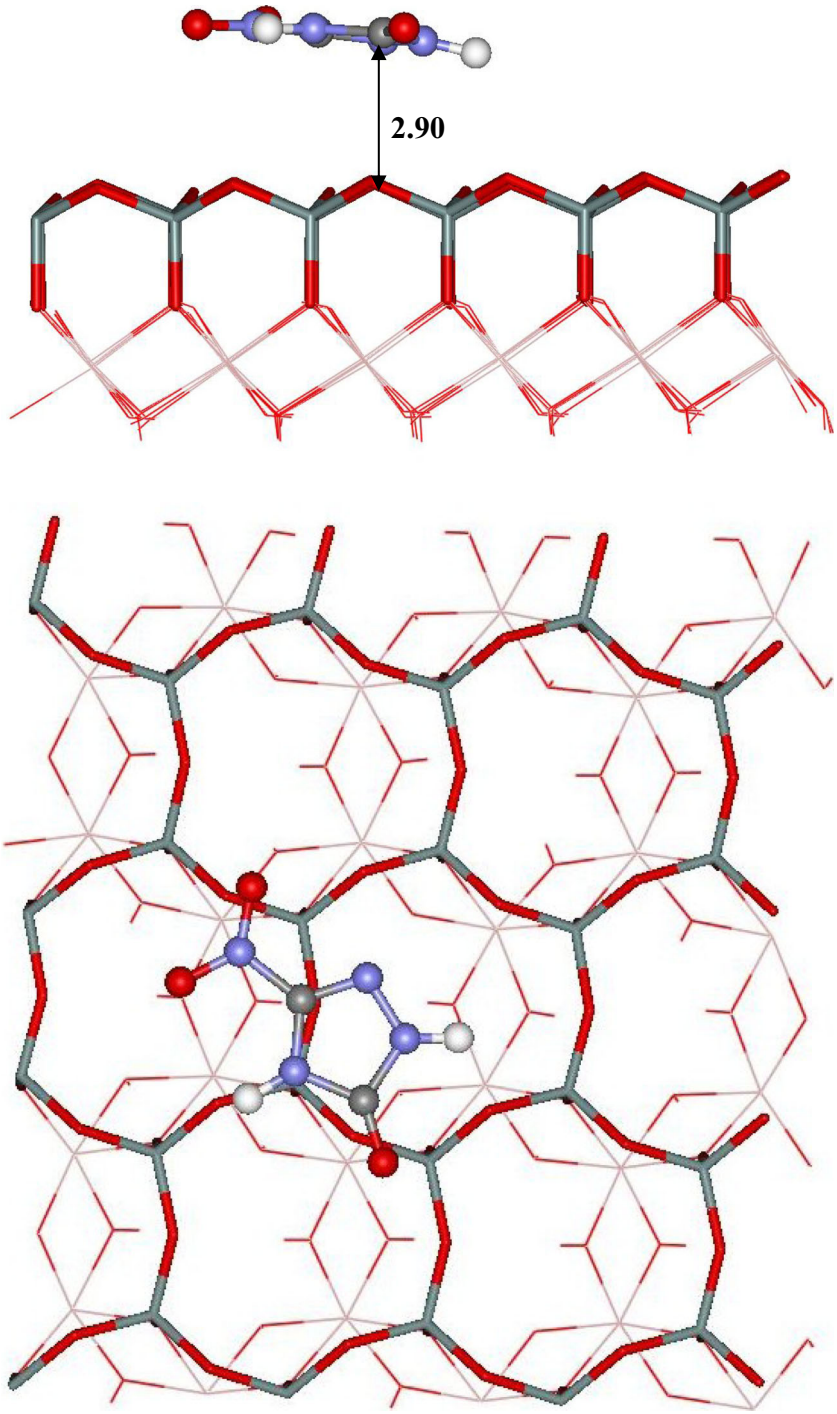

Fig. 8 Top and side view of the optimized structures of NTO adsorbed in a parallel orientation toward the tetrahedral kaolinite surface (K(t)-NTO(=)) obtained at the BLYP-D2(PBC) level of theory

regarding adsorption from aqueous solution on soil components [19, 25, 26, 63, 64]. For adsorption on metal oxide and mineral surfaces (including kaolinite) it has been shown that the presence of the solvent significantly decreases the adsorption energies [19, 25, 26, 63, 64]. The adsorption energies from aqueous solution (ΔEsol) for K-NCCs were several times lower than ΔEads, depending on the level of theory and basis set used [19]. Further, predicted adsorption strength for K(t)-NCCs in aqueous solution should be decreased since the ΔEsol values were shown to be overestimated by about 3 kcal mol^{-1} [19]. This was due to the formation of O…H-O H-bonds between NCCs and the edge OH groups of the K(t) cluster model, which do not exist in real systems. On the other hand, the presence of a sodium cation was shown to increase adsorption affinity of kaolinite toward various compounds [63, 65, 66]. Specifically, this difference amounts to 7–12 kcal mol^{-1} for NACs adsorbed on both kaolinite surfaces calculated at the M05-2X level of theory [63]. Taking into account the

Table 1 Adsorption energies (ΔEads) and BSSE values (in parentheses) [kcal mol^{-1}] and vertical distances [Å] for nitrogen containing compounds (NCCs) interacting with the octahedral (K(o)) and tetrahedral (K(t)) surface of kaolinite in the gas phase

Method model/ system	BLYP-D2 PBC	M06-2X/6-31G(d,p)[a] cluster	M06-2X/6-31+G(d,p)[a] cluster	BLYP-D2 Cluster	M06-2X-D3/6-31+G(d,p) cluster	Distance
K(o)-TNT(=)	−27.4	−26.5 (10.5)	−27.5 (8.0)	−30.7 (13.2)	−31.4 (8.0)	3.28
K(o)-DNAN(=)	−25.1	−22.9 (10.8)	−24.9 (7.4)	−28.2 (13.3)	−28.5 (7.3)	3.10
K(o)-DNT(=)	−24.3	−21.7 (8.9)	−23.6 (6.5)	−26.6 (10.9)	−26.8 (6.4)	3.07
K(o)-NTO(=)	−21.5	−26.0 (9.1)	−25.9 (6.2)	−27.7 (11.2)	−19.6 (6.2)	2.88
K(t)-TNT(=)	−13.9	−15.7 (10.9)	−15.7 (8.8)	−19.0 (11.9)	−10.6 (8.8)	3.13
K(t)-DNAN(=)	−13.7	−19.0 (10.7)	−19.1 (7.9)	−24.5 (12.1)	−14.0 (7.8)	3.06
K(t)-DNT(=)	−14.0	−16.6 (9.8)	−16.9 (7.2)	−21.3 (11.1)	−11.7 (7.1)	3.10
K(t)-NTO(=)	−12.2	−8.5 (8.2)	−10.9 (6.2)	−13.7 (9.0)	−13.8 (6.2)	2.90
K(o)-TNT(⊥)	−13.9	–	–	–	–	–
K(o)-DNAN(⊥)	−11.7	–	–	–	–	–
K(o)-DNT(⊥)	−14.3	–	–	–	–	–
K(o)-NTO(⊥)	−20.6	–	–	–	–	–
K(t)-TNT(⊥)	−3.6	–	–	–	–	–
K(t)-DNAN(⊥)	−5.5	–	–	–	–	–
K(t)-DNT(⊥)	−5.1	–	–	–	–	–
K(t)-NTO(⊥)	−10.5	–	–	–	–	–

[a] ref [19]

above mentioned facts, we fitted the BLYP-D2(PBC) ΔHads values of K(t)-NCCs(=) for adsorption on Na-kaolinite from aqueous solution. This was performed by using differences in ΔEads and ΔEsol for K(t)-NCCs(=) from our previous study [19], and differences between the kaolinite adsorption systems with and without a sodium cation. These fitted adsorption enthalpies are denoted ΔHsol, and they are presented in Table 2. As one can see, ΔHsol (−8.4 to −11.6 kcal mol^{-1}) are very close to the experimental range for NACs adsorbed on Cs^+-kaolinite (−9.6±1.2 kcal mol^{-1}) [1, 2]. A small difference can be explained by differences in the cation and experimental conditions since the adsorption strength of NACs on kaolinite was shown to significantly depend on the type of kaolinite, cation, and pH [2].

Table 2 Adsorption enthalpies [kcal mol^{-1}] for nitrogen containing compounds (NCCs) interacting with the octahedral (K(o)) and tetrahedral (K(t)) surface of kaolinite in the gas phase (ΔHads) and aqueous solution (ΔHsol)

Method model/ system	BLYP-D2[a] PBC		BLYP-D2 cluster	M06-2X-D3 cluster
	ΔHads	ΔHsol[b]	ΔHads	ΔHads
K(o)-TNT(=)	−25.0	–	−30.7	−29.4
K(o)-DNAN(=)	−23.6	–	−27.3	−26.6
K(o)-DNT(=)	−23.0	–	−26.6	−25.3
K(o)-NTO(=)	−18.9	–	−26.9	−18.0
K(t)-TNT(=)	−12.5	−11.6	−19.7	−10.0
K(t)-DNAN(=)	−12.7	−9.2	−25.1	−13.0
K(t)-DNT(=)	−12.8	−9.5	−21.9	−11.1
K(t)-NTO(=)	−9.9	−8.4	−13.5	−12.2

[a] ΔHads calculated using BLYP-D2(PBC) ΔEads and M06-2X-D3 zero point correction

[b] ΔHsol calculated from ΔHads by fitting the adsorption on kaolinite from aqueous solution in the presence of a sodium cation

Adsorption entropies and Gibbs free energies

The adsorption entropy term (ΔSads), and its contribution to the Gibbs free energies of adsorption for kaolinite-NCCs was also analyzed. Table 3 presents TΔSads values calculated at 298.15 K temperature using the M06-2X-D3 and BLYP-D2 (cluster) levels of theory for all kaolinite-NCCs systems. They are compared with the TΔSads values obtained in our previous study at the M06-2X level [19]. The TΔSads values for all

Table 3 Adsorption entropies (TΔSads) [kcal mol^{-1}] for nitrogen containing compounds (NCCs) interacting with the octahedral (K(o)) and tetrahedral (K(t)) surface of kaolinite

Method model/system	BLYP-D2 cluster	M06-2X-D3 cluster
K(o)-TNT(=)	−20.2	−18.0
K(o)-DNAN(=)	−17.5	−16.5
K(o)-DNT(=)	−18.8	−16.7
K(o)-NTO(=)	−18.8	−13.8
K(t)-TNT(=)	−19.2	−16.1
K(t)-DNAN(=)	−20.2	−16.1
K(t)-DNT(=)	−19.7	−14.2
K(t)-NTO(=)	−15.4	−14.5

kaolinite-NCCs demonstrate similar trends for both DFT functionals applied. They are in a range −13−−20 kcal mol^{-1} for both, K(o)-NCCs(=) and K(t)-NCCs(=) systems. The experimental adsorption entropy term for NACs on Cs^+-kaolinite was measured to be −7.2 kcal mol^{-1} at room temperature [2]. Since there is only a limited number of experimental adsorption entropies available, against which our calculated TΔSads values of kaolinite-NCCs can be validated, we have used the experimental adsorption entropies for various NACs interacting with zeolites and other compounds (such as stearic acid) adsorbed on kaolinite [67–73]. They are presented in Table S1 in the Supporting information. The TΔSads values for kaolinite-NCCs are more than two times greater when compared with experimental data. In our previous studies of adsorption of NCCs, benzene, and PAHs on the carbon surfaces [26, 27], the main reason for such a difference was assigned to intermolecular low-frequency modes [74–76]. Thus, we have analyzed low harmonic vibrational frequencies (below 200 cm^{-1}) for all kaolinite-NCCs(=) systems obtained using both DFT functionals. They are collected in Table S2 in the Supporting information. As one can see, all kaolinite-NCCs(=) systems are characterized by a large amount of low-frequency modes, which also include internal rotations [77]. This can be explained by the fact that during the adsorption process the conversion of translational and rotational degrees of freedom of the adsorbate molecule into low-frequency vibrations occurs [78]. In order to analyze the adsorption entropy of kaolinite-NCCs(=) more comprehensively, contributions of all three individual entropy terms (vibrational (TΔSvib), rotational TΔS(rot), and translational (TΔStrans)) were evaluated. These entropy terms are presented in Table S3 in the Supporting information. Only TΔSvib values are positive, while both TΔSrot and TΔStrans are negative, and they are several times larger than TΔSvib. They provide the major contribution to the total TΔStot term, and are mainly responsible for its large negative value. This value is overestimated for all studied kaolinite-NCCs(=) analogous as found for NCCs adsorbed on carbonaceous materials [26]. Thus, we suggest that calculations of the adsorption entropies using the harmonic oscillator approach lead to an overestimation of the rotational entropy term due to an improper treatment of internal rotations as suggested in several other studies of vibrational frequencies [77, 79, 80] and adsorption of small molecules on metal-organic frameworks [78]. To obtain more accurate Gibbs free energies of adsorption on soil components, the calculated TΔSads entropy term was divided by a factor of two to correct the entropy effect, as recommended in [26]. Gibbs free energies of adsorption (ΔGads) for all studied kaolinite-NCCs systems calculated in the gas phase at room temperature, and corrected according to this approach, are presented in Table 4.

In this section we analyze ΔGads for kaolinite-NCCs(=) systems obtained at all levels of theory (BLYP-D2(PBC), M06-2X-D3, BLYP-D2(cluster)). The BLYP-D2(PBC) ΔGads values were calculated using BLYP-D2(PBC) ΔEads, and the M06-2X-D3 zero-point correction and half TΔSads values, since the M06-2X-D3 level was shown to best mimic the PBC results. ΔGads are given in Table 4. Based on the explanation in section "Adsorption energies and enthalpies", we regard the results obtained at the BLYP-D2(PBC) level, including the ΔGads values, as the most accurate, and they will be used to make the final conclusions.

Table 4 Gibbs free energies of adsorption [kcal mol^{-1}] for nitrogen containing compounds (NCCs) interacting with the octahedral (K(o)) and tetrahedral (K(t)) surface of kaolinite in the gas phase (ΔGads) and aqueous solution (ΔGsol)

Method model/ system	BLYP-D2 PBC		BLYP-D2 cluster	M06-2X-D3 cluster
	ΔGads[a]	ΔGsol[b]	ΔGads	ΔGads
K(o)-TNT(=)	−16.0	–	−20.5	−20.4
K(o)-DNAN(=)	−15.3	–	−18.6	−18.4
K(o)-DNT(=)	−14.6	–	−17.2	−16.9
K(o)-NTO(=)	−12.0	–	−18.9	−11.1
K(t)-TNT(=)	−4.4	−3.5	−10.1	−1.9
K(t)-DNAN(=)	−4.7	−1.2	−15.0	−5.0
K(t)-DNT(=)	−5.7	−2.4	−12.1	−4.0
K(t)-NTO(=)	−2.6	−1.1	−5.8	−5.0

[a] ΔGads calculated using BLYP-D2(PBC) ΔEads and M06-2X-D3 zero point correction and half M06-2X-D3 TΔSads values

[b] ΔGsol calculated using ΔHsol and half value of TΔSads to fit the adsorption on kaolinite from aqueous solution in the presence of a sodium cation

The ΔGads values are negative for all studied kaolinite-NCCs(=). This shows that all of the studied NCCs are sufficiently stabilized on both surfaces of kaolinite to make adsorption thermodynamically feasible from the gas phase. ΔGads are much more negative for K(o)-NCCs(=) than for K(t)-NCCs(=). This corresponds with the strength of intermolecular binding as discussed in section "Geometry of adsorption complexes", which is much larger for the octahedral than tetrahedral kaolinite-NCCs complexes. The largest ΔGads value was obtained for K(o)-TNT(=) (−16.0 kcal mol^{-1}).

In order to compare calculated Gibbs free energies of K(t)-NCCs(=) with available experimental data measured in water, the ΔGads values were fitted for adsorption from aqueous solution in the presence of a sodium cation using ΔHsol predicted in section "Adsorption energies and enthalpies" and half TΔSads values (obtained at M06-2X-D3). Usage of the gas phase TΔSads values is justifiable since it was previously shown that TΔSads calculated in the gas phase and aqueous solution for adsorption on kaolinite differ only by ~1 kcal mol^{-1} [63]. Gibbs free energies of adsorption of K(t)-NCCs (=), calculated using this approach, are presented in Table 4, and they are denoted ΔGsol. We predict the BLYP-D2(PBC)

ΔGsol values for NCCs adsorbed on the siloxane site of Na^+-kaolinite from aqueous solution to be in a range from −1.1 to −3.5 kcal mol^{-1}. Taking into account the error due to the substitution of TΔSsol by TΔSads (±1 kcal mol^{-1}) [63], ΔGsol still remain negative for all K(t)-NCCs(=). This implies the effectiveness of adsorption of all calculated NCCs on Na^+-kaolinite from aqueous solution at 298.15 K. Experimental results of adsorption of NACs on kaolinite from water in the presence of cations vary in a range from 1.9 to −4.4 kcal mol^{-1} [2–4, 84–87]. Our calculated data fall into this interval. The explanation of small differences between these experimental and theoretical results is placed in the next section.

Partition coefficients

Partition coefficients (K_d) for all kaolinite-NCCs systems were calculated using the Gibbs free energies as follows:

$$K_d = \exp\left(-\frac{\Delta G}{RT}\right) \quad (1)$$

where ΔG are ΔGads and ΔGsol (presented in Table 4) obtained at all levels of theory (BLYP-D2(PBC), M06-2X-D3, BLYP-D2(cluster)), *R* is the universal gas constant, and *T* is temperature. The K_d values calculated using ΔGads or ΔGsol describe distribution of NCCs between kaolinite and air or between kaolinite and water, respectively. They were recalculated to log K_d (obtained using ΔGads), and log K_d' (obtained using ΔGsol fitted for adsorption on Na^+-kaolinite from water). They are presented in Table 5. The calculated log K_d values are positive for all studied kaolinite-NCCs systems.

Table 5 Partitioning coefficients for distribution of nitrogen containing compounds (NCCs) between octahedral (K(o)) or tetrahedral (K(t)) surface of kaolinite and air (log K_d) or water (log K_d')

Method model/ system	BLYP-D2 PBC		BLYP-D2 cluster	M06-2X-D3 cluster
	Log K_d[a]	Log K_d'[b]	Log K_d[a]	Log K_d[a]
K(o)-TNT(=)	11.7	–	15.0	15.0
K(o)-DNAN(=)	11.2	–	13.6	13.4
K(o)-DNT(=)	10.7	–	12.6	12.4
K(o)-NTO(=)	8.8	–	13.9	8.1
K(t)-TNT(=)	3.2	2.6	7.4	1.4
K(t)-DNAN(=)	3.4	0.9	11.0	3.6
K(t)-DNT(=)	4.2	1.8	8.8	2.9
K(t)-NTO(=)	1.9	0.8	4.2	3.6

[a] Log K_d calculated from ΔGads

[b] Log K_d' calculated from ΔGsol to fit the adsorption on kaolinite from aqueous solution in the presence of a sodium cation

They vary from 8.1 to 15.0 for K(o)-NCCs(=), and from 1.9 to 11.0 for K(t)-NCCs(=). Experimental log K_d for distribution of various environmental contaminants, including PAHs, between air and soil are in a range 3.2–12.8 (9.1–12.3 for PAHs) [62, 81–83]. Our predicted BLYP-D2(PBC) log K_d values, which we regard as the most accurate, generally belong to this experimentally measured interval. As expected, calculated log K_d for TNT, DNT, and DNAN adsorbed on K(o) are slightly higher than experimental log K_d for PAHs since NACs were shown to more strongly adsorb to soil components than PAHs [25, 26].

A few experimental studies were published, in which partition coefficients were measured for distribution of NACs between water and kaolinite in the presence of cations [2–4, 84–87]. Experimental log K_d' vary between -1.4 and 3.2 [84–87]. To the best of our knowledge, in only one report log K_d' was measured for adsorption of TNT on untreated kaolinite from aqueous solution (-0.7) [87]. Our calculated BLYP-D2(PBC) log K_d' for K(t)-NCCs, which characterize adsorption on Na^+-kaolinite from aqueous solution (see Table 5), vary from 0.8 to 2.6. These values fall into the experimentally measured range. Small discrepancy of theoretical and experimental data can be caused by differences in experiments and calculated models such as impurities, small surface charge differences, and the presence of different cations in solution. The latter has been shown to have a significant effect on the K_d values for adsorption of TNT on kaolinite. The log K_d' value for TNT adsorbed on Ca^{2+}-saturated kaolinite was measured to be much lower (-1) than the values observed for kaolinite saturated with K^+ (0.7) and NH_4^+ (0.4) [87]. Moreover, our simple model of adsorption of NCCs on the siloxane surface of Na^+-kaolinite in water does not take into account such factors as solubility, nitroreduction, and competition with water, which are expected to play an important role in the adsorption process [18]. Thus, at the kaolinite–water interface, the influence of the above listed factors can result in smaller experimental log K_d' values. Further investigations are needed to better understand the phenomenon of adsorption from aqueous solution in the presence of cations with a construction of the surface models that take into account all of the parameters described above.

Conclusions

M06-2X and B3LYP DFT functionals with inclusion of D2 and D3 dispersion terms and both, periodic and cluster approaches were applied to investigate adsorption of nitrogen containing compounds (NCCs, 2,4,6, trinitrotoluene (TNT), 2,4-dinitrotoluene (DNT), 2,4-dinitroanisole (DNAN), and 3-one-1,2,4-triazol-5-one (NTO)). The M06-2X-D3(cluster) adsorption energies were shown better mimic the BLYP-D2

(periodic) data than the BLYP-D2(cluster) results. Binding of studied NCCs was found to be almost two times greater with the octahedral than with tetrahedral surface of kaolinite. All studied NCCs were preferably adsorbed in a parallel than perpendicular orientation on both kaolinite surfaces. TNT was the most strongly adsorbed on the octahedral surface of kaolinite, and NTO was the least strongly adsorbed on both kaolinite surfaces among studied NCCs.

The main focus of this study was prediction of thermodynamic parameters for adsorption of NCCs on kaolinite from the gas phase. The results reveal the effectiveness of adsorption for all NCCs on both kaolinite surfaces from the gas phase at room temperature. Adsorption enthalpies for kaolinite-NCCs obtained at all levels of theory were shown to be quite accurate when compared with published experimental data for various environmental contaminants, including nitroaromatics on kaolinite. The Gibbs free energies and partition coefficients were also computationally estimated and validated against previously published experimental data for NCCs on kaolinite from aqueous solution. We suggest that all studied NCCs will form stable surface complexes with Na-kaolinite in aqueous solution at 298.15 K. The presence and type of cations and impurities were shown to have a significant effect of the strength of adsorption and the process of distribution of NCCs between kaolinite and water.

Acknowledgments This work was facilitated by support from the High Performance Computing Distributed Shared Resource Center at the ERDC (Vicksburg, MS). The use of trade, product, or firm names in this report is for descriptive purposes only and does not imply endorsement by the U.S. Government. Results in this study were funded and obtained from research conducted under the Environmental Quality Technology Program of the United States Army Corps of Engineers by the US Army ERDC. Permission was granted by the Chief of Engineers to publish this information. The findings of this report are not to be construed as an official Department of the Army position unless so designated by other authorized documents.

References

1. Weissmahr KW, Haderlein SB, Schwarzenbach RP, Hany R, Nüesch R (1997) Environ Sci Technol 31:240–247
2. Haderlein SB, Schwarzenbach RP (1993) Environ Sci Technol 27: 316–326
3. Haderlein SB, Weissmahr KW, Schwarzenbach RP (1996) Environ Sci Technol 30:612–622
4. Weissmahr KW, Haderlein SB, Schwarzenbach RP (1998) Soil Sci Soc Am J 62:369–378
5. Weissmahr KW, Hildenbrand M, Schwarzenbach RP, Haderlein SB (1999) Environ Sci Technol 33:2593–2600
6. Boyd SA, Sheng G, Teppen BJ, Johnston CT (2001) Environ Sci Technol 35:4227–4234
7. Johnston CT, de Oliveira MF, Teppen BJ, Sheng G, Boyd SA (2001) Environ Sci Technol 35:4767–4772
8. Takenawa R, Komori Y, Hayashi S, Kawamata J, Kuroda K (2001) Chem Mater 13:3741–3746
9. Michalkova A, Szymczak JJ, Leszczynski J (2005) Struct Chem 16: 325–337
10. Wang X, Qian P, Song K, Zhang C, Dong J (2013) Comput Theor Chem 1025:16–23
11. Gorb L, Gu J, Leszczynska D, Leszczynski J (2000) Phys Chem Chem Phys 2:5007–5012
12. Pelmenschikov A, Leszczynski J (1999) J Phys Chem B 103:6886–6890
13. Gorb L, Lutchyn R, Zub Y, Leszczynska D, Leszczynski J (2006) J Mol Struc-THEOCHEM 766:151–157
14. Newman ACD (1987) Chemistry of clays and clay minerals. Longman, London
15. Bailey SW (1980) Crystal structures of clay minerals and their X-ray identification. Mineralogical Society, London
16. Young RA, Hewat AW (1988) Clays Clay Miner 36:225–232
17. Alzate LF, Ramos CM, Herna´ndez NM, Herna´ndez SP, Mina N (2006) Vib Spectrosc 42:357–368
18. Hurley MM, Paul KW (2009) Environmental fate and transport of energetic materials. In: DoD High Performance Computing Modernization Program Users Group Conference (HPCMP-UGC) IEEE, pp 186−189
19. Scott AM, Burns EA, Hill FC (2014) J Mol Model 20:2373–2377
20. Tsendra O, Scott AM, Gorb L, Boese AD, Hill FC, Ilchenko MM, Leszczynska D, Leszczynski J (2014) J Phys Chem 118(6):3023–3034
21. Bell AT, Head-Gordon M (2011) Annu Rev Chem Biomol Eng 2: 453–477
22. Efremenko I, Sheintuch M (2006) Langmuir 22:3614–3621
23. Fara D, Kahn I, Maran U, Karelson M, Andersson P (2005) J Chem Inf Model 45:94–105
24. Kubicki JD (2006) Environ Sci Technol 40:2298–2303
25. Michalkova A, Gorb L, Hill F, Leszczynski J (2011) J Phys Chem A 115:2423–2430
26. Scott AM, Gorb L, Mobley EA, Hill FC, Leszczynski J (2012) Langmuir 28:13307–13317
27. Scott AM, Gorb L, Burns EA, Yashkin SN, Hill FC, Leszczynski J (2014) J Phys Chem C 118(9):4774–4783
28. Neder RB, Burghammer M, Grasl TH, Schulz H, Bram A, Fiedler S (1999) Clays Clay Miner 47:487–494
29. Kremleva A, Krüger S, Rösch N (2008) Langmuir 24:9515–9524
30. Lee SG, Choi JI, Koh W, Jang SS (2013) Appl Clay Sci 71:73–81
31. Benco L, Tunega D, Hafner J, Lischka H (2001) Chem Phys Lett 333:479–484
32. Benco L, Tunega D, Hafner J, Lischka H (2001) Am Mineral 86: 1057–1065
33. Benco L, Tunega D, Hafner J, Lischka H (2001) J Phys Chem B 105: 10812–10817
34. Hutter J (1997) CPMD 3.0. Copyright IBM Corporation 1990−1997 and MPI Festkörperforschung, Stuttgart
35. Becke AD (1988) Phys Rev A 38:3098–3100
36. Lee C, Yang W, Parr RG (1988) Phys Rev B 37:785–789
37. Grimme S (2006) J Comp Chem 27:1787–1799
38. Goedecker S, Teter M, Hutter J (1996) Phys Rev B 54:1703–1710
39. Hartwigsen C, Goedecker S, Hutter J (1998) Phys Rev B 58:3641–3662
40. Parr RG, Yang W (1989) Density-functional theory of atoms and molecules. Oxford University Press, Oxford
41. Frisch MJ, Trucks GW, Schlegel HB, Scuseria GE, Robb MA, Cheeseman JR, Scalmani G, Barone V, Mennucci B, Petersson GA, Nakatsuji H, Caricato M, Li X, Hratchian HP, Izmaylov AF, Bloino J, Zheng G, Sonnenberg JL, Hada M, Ehara M, Toyota K, Fukuda R, Hasegawa J, Ishida M, Nakajima T, Honda Y, Kitao O, Nakai H, Vreven T, Montgomery JA Jr, Peralta JE, Ogliaro F, Bearpark M, Heyd JJ, Brothers E, Kudin KN, Staroverov VN, Kobayashi R, Normand J, Raghavachari K, Rendell A, Burant JC, Iyengar SS, Tomasi J, Cossi M, Rega N, Millam JM, Klene M, Knox JE, Cross

JB, Bakken V, Adamo C, Jaramillo J, Gomperts R, Stratmann RE, Yazyev O, Austin AJ, Cammi R, Pomelli C, Ochterski JW, Martin RL, Morokuma K, Zakrzewski VG, Voth GA, Salvador P, Dannenberg JJ, Dapprich S, Daniels AD, Farkas Ö, Foresman JB, Ortiz JV, Cioslowski J, Fox DJ (2009) Gaussian 09, Revision A.1. Gaussian Inc, Wallingford
42. Zhao Y, Schultz NE, Truhlar DG (2006) J Chem Theory Comput 2: 364–382
43. Grimme S, Antony J, Ehrlich S, Krieg HA (2010) J Chem Phys 132: 154104–154122
44. Boys SF, Bernardi F (1970) Mol Phys 19:553–566
45. Shukla MK, Hill F (2014) J Phys Chem C 118:310–319
46. Shukla MK, Hill F (2013) J Phys Chem C 117:13136–13142
47. Castro EAS, Martins JBL (2005) Int J Quantum Chem 103:550–556
48. Castro EAS, Gargano R, Martins JBL (2012) Int J Quantum Chem 112:2828–2831
49. Michalkova A, Robinson TL, Leszczynski J (2011) Phys Chem Chem Phys 13:7862–7881
50. Zhanpeisov NU, Adams JW, Larson SL, Weiss CA Jr, Zhanpeisova BZ, Leszczynska D, Leszczynski J (1999) Struct Chem 10:285–294
51. Abbasi A, Nadimi E, Plänitz P, Radehaus C (2009) Surf Sci 603: 2502–2506
52. Piane MD, Corno M, Ugliengo P (2013) J Chem Theory Comput 9: 2404–2415
53. Mian SA, Saha LC, Jang J, Wang L, Gao X, Nagase S (2010) J Phys Chem C 114:20793–20800
54. Rimola A, Civalleri B, Ugliengo P (2010) Phys Chem Chem Phys 12:6357–6366
55. Rimola A, Sodupe M, Ugliengo P (2009) J Phys Chem C 113:5741–5750
56. Van der Mynsbrugge J, Hemelsoet K, Vandichel M, Waroquier M, Van Speybroeck V (2012) J Phys Chem C 116:5499–5508
57. Flick JC, Kosenkov D, Hohenstein EG, Sherrill CD, Slipchenko LV (2012) J Chem Theory Comput 8:2835–2843
58. Kang R, Chen H, Shaik S, Yao J (2011) J Chem Theory Comput 7: 4002–4011
59. Biswal HS, Gloaguen E, Mons M, Bhattacharyya S, Shirhatti PR, Wategaonkar S (2011) J Phys Chem A 115:9485–9492
60. Goerigk L, Kruse H, Grimme S (2011) Chem Phys Chem 12:3421–3433
61. He X, Chen S, Quan X, Liu Z, Zhao Y (2009) Chemosphere 77: 1427–1433
62. Meijer SN, Shoeib M, Jones KC, Harner T (2003) Environ Sci Technol 37:1300–1305
63. Scott AM, Dawley MM, Orlando TM, Hill FC, Leszczynski J (2012) J Phys Chem C 116:23992–24005
64. Aquino AJA, Tunega D, Haberhauer G, Gerzabek MH, Lischka H (2003) J Comput Chem 24:1853–1863
65. Clausen P, Andreoni W, Curioni A, Hughes E, Plummer CJG (2009) J Phys Chem C 113:15218–15225
66. Mignon P, Ugliengo P, Sodupe M (2009) J Phys Chem C 113:13741–13749
67. Denayer JF, Baron GV, Martens JA, Jacobs PA (1998) J Phys Chem B 102:3077–3081
68. Ocakoglu RA, Denayer JFM, Marin GB, Martens JA, Baron GV (2003) J Phys Chem B 107:398–406
69. Tielens F, Denayer JFM, Daems I, Baron GV, Mortier WJ, Geerlings P (2003) J Phys Chem B 107:11065–11071
70. De Moor BA, Reyniers M-F, Gobin OC, Lercher JA, Marin GB (2010) J Phys Chem C 115:1204–1219
71. Boulard S, Gilot P, Brosius R, Habermacher D, Martens JA (2004) Top Catal 30:49–53
72. Valenzano L, Civalleri B, Chavan S, Palomino GT, Arean CO, Bordiga S (2010) J Phys Chem C 114:11185–11191
73. Sari A, Ipyldak O (2006) Bull Chem Soc Ethiop 20:259–267
74. Hobza P, Bludsky O, Suhai S (1999) Phys Chem Chem Phys 1:3073–3078
75. Barone V (2005) J Chem Phys 122:014108–014117
76. Wang W, Pitonak M, Hobza P (2007) Chem Phys Chem 8:2107–2111
77. Ayala PY, Schlegel HB (1998) J Chem Phys 108:2314–2325
78. Sillar K, Sauer J (2012) J Am Chem Soc 134:18354–18365
79. Barone V (2004) J Chem Phys 120:3059–3065
80. Ben-Tal N, Honig B, Bagdassarian CK, Ben-Shaul A (2000) Biophys J 79:1180–1187
81. Hippelein M, Mclachlan MS (1998) Environ Sci Technol 32:310–316
82. Cabrerizo A, Dachs J, Jones KC, Barcel´ D (2011) Atmos Chem Phys 11:12799–12811
83. Ribes S, Van Drooge B, Dachs J, Gustafsson Ø, Grimalt JO (2003) Environ Sci Technol 37:2675–2680
84. Pichtel J (2012) Appl Environ Soil Sci 2012:1–33
85. Cattaneo MV, Pennington JC, Brannon JM, Gunnison D, Harrelson DW, Zakikhani M (2000) Natural attenuation of explosives in remediation of hazardous waste contaminated soils. Dekker, New York
86. Caulfield JA (2008) Analytical studies of sorption phenomena for nitrogen heterocycles. Dissertation, http://digitaldu.coalliance.org/fedora/repository/codu%3A63047/ETD_umi-denver-1018.pdf-0/master
87. Price CB, Brannon JM, Yost SL, Hayes CA (2000) Adsorption and transformation of explosives in low-carbon aquifer soils. Technical Report, ERDC/EL TR-00-11. U.S. Army Engineer Research and Development Center, Vicksburg, MS